International Atomic Energy Agency

INDC(GDR)-055/LJ

INDC INTERNATIONAL NUCLEAR DATA COMMITTEE

GLOBAL DESCRIPTION OF (n,p) - AND (n,2n) - ACTIVATION CROSS SECTIONS WITHIN STATISTICAL MULTISTEP THEORY

H. Kalka[1], M. Torjman[1], H.N. Lien[2], R. Lopez[3], and D. Seeliger[1]

1 Technische Universität Dresden, Sektion Physik, Dresden 8027, GDR
2 National Atomic Energy Institute, 67 Nguyen Du, Hanoi, Vietnam
3 Institute of Nuclear Science and Technology, P.O. Box 6122, Habana, Cuba

July 1989

IAEA NUCLEAR DATA SECTION, WAGRAMERSTRASSE 5, A-1400 VIENNA

INDC(GDR)-055/LJ

GLOBAL DESCRIPTION OF (n,p) - AND (n,2n) - ACTIVATION CROSS SECTIONS WITHIN STATISTICAL MULTISTEP THEORY

H. Kalka[1], M. Torjman[1], H.N. Lien[2], R. Lopez[3], and D. Seeliger[1]

1 Technische Universität Dresden, Sektion Physik, Dresden 8027, GDR
2 National Atomic Energy Institute, 67 Nguyen Du, Hanoi, Vietnam
3 Institute of Nuclear Science and Technology, P.O. Box 6122, Habana, Cuba

July 1989

Reproduced by the IAEA in Austria
July 1989

89-02910

Global Description of (n,p) - and (n,2n) - Activation Cross Sections within Statistical Multistep Theory

H. Kalka[1], M. Torjman[1], H. N. Lien[2], R. Lopez[3], and D. Seeliger[1]

[1] Technische Universität Dresden, Sektion Physik, Dresden 8027, G.D.R.

[2] National Atomic Energy Institute, 67 Nguyen Du, Hanoi, Vietnam

[3] Institute of Nuclear Science and Technology, P.O. Box 6122, Habana, Cuba

Abstract

A unique description of (n,p) and (n,2n) activation cross sections as well as emission spectra is proposed within a pure multistep approach. Calculations are presented for 8 nuclei (A=47...65) in the incident energy range from zero up to 20 MeV.

I. Introduction

In the last years it becomes customary to describe activation cross-sections induced by fast neutrons in the frame of statistical (Hauser-Feshbach) plus preequilibrium emission models [1-4]. Usually in this procedure two parameter sets were adopted which (strongly) variate from nucleus to nucleus. It is the purpose of the present work to improve this situation, but within a pure statistical multistep approach [5,6]. This approach bases on random matrix physics [7,8] and was derived from Green's function formalism [9] in [6,10,11]. It contains both statistical multistep direct (SMD) and multistep compound (SMC) processes. The SMC-description also was adopted for multiple particle emission (MPE) reactions (e.g., (n,2n), (n,np), ...).

In previous papers [6,10,11] it was shown that the SMD/SMC model is succesfull in reproducing neutron and proton emission spectra (and angular distributions) at incident energies between 5 and 26 MeV but, a discussion of excitation functions was still missing. Now a bulk of numerical calculations was carried out to propose a systematical way in solving the latter problem. Some typical examples (^{47,48}Ti, ^{52}Cr, ^{56}Fe, ^{58,60}Ni, ^{59}Co, ^{65}Cu) will be presented in Sect.3.

The route taken here differs from other evaluations in two respects:
First, it is a *global* description since all calculations are performed with global parameters (single-particle state density g=A/13; global optical model potentials; residual interaction strength V_0=19.4 MeV; etc.).
Second, it could be called a *standard* or *minimum* description since to make the calculations transparent besides Pauli exlusion principle all other corrections (exact shell-structure; refined pairing models; renormalization of state densities; two-component approach; etc.) are ignored. Also angular momentum and parity conservations are not taken into account.

Hence, differences between calculated and experimental data give us a measure for deviations from an average nuclear behaviour. Starting from the standard version later on higher-order effects listed above should be studied.

Besides several recent improvements of the model the main difference between these results and those given in our previous papers consist in the definition of binding energies. Whereas for

SMD-calculations always the exact (i.e. experimental) binding energies B are used the SMC-calculations (including MPE) are performed with liquid drop binding energies,

$$B^{LD} = \begin{cases} B+\Delta \\ B-\Delta \end{cases} \text{ in } \begin{matrix} \text{odd} \\ \text{even} \end{matrix} \text{ systems .} \tag{1}$$

Here, the fluctuating energy-shift Δ contains pairing and shell-structure corrections. But, as obvious from mass tables [12] it can be approximated fairly-well by a constant $\Delta = 12.8 \; A^{-1/2}$ (in MeV) taken from [13].

Before presenting the results in Sect.3 the model in its standard version will be reported briefly in Sect.2. Notice that the SMD-part is modiefied in comparison with [5]. Also the SMC-formulas (escape widths) given in [5,6] are simplified in this paper.

II. The model

In our statistical multistep model the total emission spectrum of the process (a,xb) is devided in three main parts,

$$\frac{d\sigma_{a,xb}(E_a)}{dE_b} = \frac{d\sigma_{ab}^{SMD}(E_a)}{dE_b} + \frac{d\sigma_{ab}^{SMC}(E_a)}{dE_b} + \frac{d\sigma_{a,xb}^{MPE}(E_a)}{dE_b} \quad . \tag{2}$$

The first term denotes the statistical multistep direct part and contains one- and two-step contributions. The second term symbolizes the multistep compound emission. Both terms together represent the so-called first-chance emission process. Otherwise, the second-chance, third-chance emissions, etc. are summarized in the last term, i.e.,

$$\frac{d\sigma^{MPE}_{a,xb}(E_a)}{dE_b} = \sum_c \frac{d\sigma_{a,cb}}{dE_b} + \sum_{c,d} \frac{d\sigma_{a,cdb}}{dE_b} + \ldots \quad . \tag{3}$$

In this paper we restrict ourselves to particle-type indices a,b,...= n, p or γ which denote neutron, proton, and γ-ray.

The following (model-independent) relations between the optical-model (OM) reaction cross section and the energy-integrated partial cross sections should be satisfied (at incident energy E_a)

$$\sigma^{OM}_a = \sum_b \sigma_{a,b} \quad , \tag{4a}$$

$$\sigma_{a,b} = \sum_c \sigma_{a,bc} \quad \text{and} \quad \sigma_{a,bc} = \sum_d \sigma_{a,bcd} \ , \quad \text{etc.} \tag{4b}$$

with $\sigma_{a,b} = \sigma^{SMD}_{ab} + \sigma^{SMC}_{ab}$ as the total first-chance emission cross section. In this context, activation cross sections are given by

$$\sigma_{a,b\gamma} = \sigma_{a,b} - \sum_{c\neq\gamma} \sigma_{a,bc} \tag{5a}$$

$$\sigma_{a,cb\gamma} = \sigma_{a,cb} - \sum_{d\neq\gamma} \sigma_{a,cbd} \tag{5b}$$

where b,c,d $\neq \gamma$. More explicitly, the (n,p)- and (n,2n)-excitation functions have the form

$$\sigma_{n,p\gamma} = \sigma_{n,p} - \sigma_{n,pn} - \sigma_{n,2p} \quad , \tag{6a}$$

$$\sigma_{n,2n\gamma} = \sigma_{n,2n} - \sigma_{n,3n} - \sigma_{n,2np} \quad . \tag{6b}$$

2.1. SMD cross section

For the incident-energy range below 20 MeV we restrict ourselves to one- and two-step contributions since the SMD process

terminates after few collisions. According to the distinction between non-collective particle-hole excitations [ex] and collective vibrational states [vib] the SMD cross section becomes a sum of 2 one-step and 4 two-step contributions,

$$\frac{d\sigma_{ab}^{SMD}(E_a)}{dE_b} = \sum_{[\alpha]} \left[\frac{m\mathcal{V}}{2\pi\hbar^2} \right]^2 \frac{4\pi}{(k_a R)^2} [\ \alpha\ ] \frac{k_b}{k_a} \mathcal{P}_a(E_a)\mathcal{P}_b(E_b) \tag{7}$$

where [α] symbolizes the individual contributions denoted according to the sequence of exciton and phonon excitations,

$$[ex] = \mathcal{R}_{ab}\ (V_o A^{-4/3} g)^2\ U \tag{8a}$$

$$[vib] = \delta_{ab} \sum_{\lambda} \hat{\beta}_\lambda^2\ V_R^2\ \delta(U-\omega_\lambda) \tag{8b}$$

as well as [2ex], [ex,vib], [vib,ex], and [2vib]. The analytical expressions of the latter are reported in [6].

The following abbreviations are used: $U=E_a+B_a-B_b-E_b$ is the residual excitation energy; B_c and $E_c=\hbar^2 k_c^2/2m$ are the binding and kinetic energies. V_o is the strength of the residual (surface-delta) interaction,

$$V(r_1-r_2) = -\ V_o\ \frac{4\pi}{3}\ r_o^4\ \delta(r_1-r_2)\ \delta(r_1-R)\ . \tag{9}$$

In (8b) the real OM potential depth is denoted by V_R. Otherwise, the quantities ω_λ and $\beta_\lambda^2 = 4\pi(2\lambda+1)\hat{\beta}_\lambda^2$ denote the energy and deformation parameter of a phonon with multipolarity λ. The combinatorial factor is given by

$$\mathcal{R}_{ab}A^2 = \delta_{ab}\ (N^2+Z^2) + (1-\delta_{ab})\ (N^2\delta_{bn}+Z^2\delta_{bp})\ . \tag{10}$$

Further, the quantity

$$\rho(E_c) = \frac{4\pi\ \mathcal{V}\ mk_c}{(2\pi)^3\hbar^2} \tag{11}$$

is the single-particle state density in the nucleus volume $\mathcal{V}= 4\pi R^3/3$ and $R = r_0 A^{1/3}$. At Fermi energy E_F=40 MeV and for r_0=1.40 fm it takes the value $2(2s+1)\rho(E_F) \equiv g = A/13$ (in MeV^{-1}). Finally, the penetration factors are given by

$$\mathcal{P}_c(E_c) = \delta_{cn} + [\ \sigma_p^{OM}(E_c)\ /\ \sigma_n^{OM}(E_c)\ ]\ \delta_{cp}\ . \qquad (12)$$

All SMD-calculations are performed with the following parameters: V_R= 48 MeV, V_0= 19.4 MeV (obtained from the OM reaction cross section in [6]), r_0=1.40 fm, and g=A/13. In case of phonon excitations we restrict ourselves to two low-lying vibrational states of multipolarity $\lambda^\pi = 2^+$ and 3^-. For odd-mass nuclei the weak coupling model [14] was adopted. The values of ω_2, β_2 and ω_3 are taken from [14-16] whereas for $\lambda = 3$ the parametrization $\beta_\lambda^2 = (2\lambda+1)\omega_\lambda/(2C_\lambda)$ with C_3= 500 MeV was used (see Table 1). All delta functions entering (8b) are replaced by Gaussians of width 0.7 MeV simulating both the limited (exit channel) energy resolution in experiments and the spreading of spectroscopic strength.

One additional note is necessary concerning a constant pairing shift $\Delta = 12.8\ A^{-1/2}$. Whereas it is ignored for $\sigma_{n,n'}^{SMD}$ completely in case of charge-exchange processe, $\sigma_{n,p}^{SMD}$, we use U-Δ for odd-mass targets only. This was found from comparison between calculated and experimental proton emission spectra (n,xp) at 14 MeV for several nuclei (^{65}Cu, ^{93}Nb, ^{107}Ag, ^{115}In). Otherwise, in case of even-even targets we have an odd-odd residual nucleus and, hence, it gives no rise for a pairing shift.

Table 1 Binding energies as well as energies and deformation parameters of two low-lying phonon states of multipolarity 2^+ and 3^-

Target	B_n/MeV	B_p/MeV	ω_2/MeV	β_2	ω_3/MeV	β_3
^{47}Ti	11.62	11.45	0.889	0.317	3.05	0.146
^{48}Ti	8.14	11.35	0.983	0.269	3.36	0.153
^{52}Cr	7.94	11.13	1.434	0.224	4.59	0.179
^{56}Fe	7.67	10.56	0.847	0.239	4.52	0.178
^{58}Ni	9.00	8.60	1.454	0.183	4.47	0.177
^{59}Co	7.07	8.42	1.346	0.179	3.70	0.161
^{60}Ni	7.82	9.86	1.332	0.207	4.00	0.168
^{65}Cu	7.49	8.82	1.330	0.207	4.05	0.168

2.2. SMC cross section

The SMC cross section has the familiar form

$$\frac{d\sigma_{ab}^{SMC}(E_a)}{dE_b} = \sigma_a^{SMC}(E_a) \sum_m \frac{\tau_m}{\hbar} \Gamma_{mb}(E_b)\uparrow \tag{13}$$

where τ_m satisfies the time-integrated master equation

$$-\hbar\,\delta_{mm_o} = \Gamma^{(+)}_{m-2\downarrow}\,\tau_{m-2} + \Gamma^{(-)}_{m+2\downarrow}\,\tau_{m+2} - \Gamma_m\tau_m \tag{14}$$

for each exciton number m=p+h. The sum runs from m_o=3 up to $(2gE)^{1/2}$ which includes the equilibrium stage $\bar{m} \simeq (1.4gE)^{1/2}$. Here, $E=E_a+B_a^{LD}$ is the excitation energy of the composite system. (Note, there is no double-counting of emissions from exciton states m=3 and 5 in SMD and SMC processes. It is, because in SMD

processes we only consider diagrams of particle-hole creation by scattering of *particles*. On the other hand, the SMC emission with pair-creation contains only diagrams of *hole*-scattering. The latter is described in (17a) below.)

In (14) the damping widths are given by

$$\Gamma_m^{(\Delta m)}\downarrow = 2\pi\ (V_o/A)^2\ \rho_m^{(\Delta m)}(E)\ . \tag{15}$$

The final state densities of the *composite* system, $\rho_m^{(\Delta m)}(E)$, are reported in [6]. They differ from those given in [17] by the inclusion of a correction for Pauli-principle $A_{ph}=(p^2+h^2+p-3h)/4g$.

For the (differential) escape widths we have (b = neutron and/or proton)

$$\Gamma_{mb}(E_b)\uparrow = 2\pi\ (V_o/A)^2\ (2s+1)\ \rho(E_b)\ \mathcal{P}_b(E_b) \sum_{\Delta m} \rho_m^{(\Delta m)}(U) \tag{16}$$

where the sum runs over three escape modes defined by the final state density of the *residual* system,

$$\rho_m^{(+)}(U) = \frac{h}{m}\, g^2\ E_{ph} \left(\frac{U_{p,h+1}}{E_{ph}} \right)^n \tag{17a}$$

$$\rho_m^{(0)}(U) = p(h+\frac{p-1}{2})g \left(\frac{U_{p-1,h}}{E_{ph}} \right)^{n-2} \left[(m-1)-(m-2)\left(\frac{U_{p-1,h}}{E_{ph}} \right)\right] \tag{17b}$$

$$\rho_m^{(-)}(U) = \frac{p(p-1)h}{4E_{ph}}\ \frac{(m-1)!}{(m-4)!} \left(\frac{U_{p-2,h-1}}{E_{ph}}\right)^{n-4} \left[1-\left(\frac{U_{p-2,h-1}}{E_{ph}}\right)\right]^2 . \tag{17c}$$

Here, for the (Pauli-corrected) excitation energies of the composite and residual systems the abbreviations

$$E_{ph} = E - A_{ph}\ , \tag{18a}$$

$$U_{ph} = E - A_{ph} - B_b^{LD} - E_b \tag{18b}$$

are used. If, for example, the Pauli-correction A_{ph} would be ignored, then the final state densities in (17) turn to those proposed in [17]. Note, however, the factor h/m in (17a) which excludes pair-creation by particle-scattering.

In contrat to the refined accounting of pairing effects in [6] this problem is now approximated by using liquid drop binding energies (1). However, in order to guarantee that the maximum emission energy in emission spectra should not be overpredicted (which, in some cases, holds by using B^{LD}) it is necessary to multiply the escape widths (16) by a step-function $\Theta(E_a+B_a-B_b-E_b)$.

Finally, the total width in (14) is defined by

$$\Gamma_m = \Gamma_m^{(+)}\downarrow + \Gamma_m^{(-)}\downarrow + \sum_b \int dE_b\, \Gamma_{mb}(E_b)\uparrow \quad . \tag{19}$$

According to (4a) the normalization constant in (13) is chosen as

$$\sigma_a^{SMC}(E_a) = \sigma_a^{OM}(E_a) - \sum_b \sigma_{a,b}^{SMD}(E_a) - \sigma_{a,\gamma}(E_a) \quad . \tag{20}$$

The last term in (20) occures since there are no escape widths for γ-emission in (19) so far. However, for incident energies above a few MeV the capture process (a,γ) is very small, $\sigma_{a,\gamma} \ll \sigma_a^{OM}$, and we put $\sigma_{a,\gamma}(E_a) \equiv 0$.

Again, it is remarkable that the quantity V_o^2 entering the widths in (15) and (16) cancel within the sum of (13). Thus, in this approximation the SMC emission becomes independent of the residual interaction strength V_o.

2.3. MPE cross section

The MPE is treated as a pure SMC approach. Hence, we use (13), but it should be modified in two respects. (In this paper we consider second-chance processes (a,cb) only. An extension to higher-chance emission processes is straigthforward.)

First, the (liquid drop) binding energy B_b^{LD} in (18b) should be replaced by

$$B_b^{LD} \longrightarrow B_b^{MPE} \equiv B_c^{LD} + B_{cb}^{LD} + (B_a^{LD} - B_a) \tag{21}$$

which gives for the residual energy

$$\begin{aligned} U_{ph} &= E_{ph} - B_b^{MPE} - E_b \\ &= E_a + B_a - A_{ph} - B_c^{LD} - B_{cb}^{LD} - E_b \, . \end{aligned} \tag{22}$$

The quantity B_{cb}^{LD} indicates the (liquid drop) binding energy of particle b (after emission of particle c) in the nuclear system (A-c). Equation (22) looks very similar to older evaporation models for MPE if the quantity A_{ph} will be replaced by $\bar{E}_c$ which is the mean emission-energy shift of the previous emitted particle. Indeed, both values coincide nearly, $A_{\bar{p}\bar{h}} \simeq \bar{E}_c$, for particle and hole numbers at equilibrium stage $\bar{m}$. (At incident energies around 14 MeV it takes the value 2.5 MeV for $A \simeq 60$.)

Second, the normalization constant in (13) should be replaced (according to (5a)) by

$$\sigma_a^{SMC} \longrightarrow \sigma_{a,c}^{MPE} \equiv \sum_{b \neq \gamma} \sigma_{a,cb} = \sigma_{a,c} - \sigma_{a,c\gamma} \tag{23}$$

at incident energy E_a. In contrast to the first-chance process

(a,γ) the γ-emission process (a,cγ) can not been ignored. The latter will be approximated by a sharp cut-off model where γ-emission occures below neutron threshold only, and above this threshold γ-competition is ignored. More explicitly, we use

$$\sigma_{n,n'\gamma}(E_n) = \sigma^{SMD}_{nn'} + \int_{x_1}^{E_n} dE_{n'} \left[\frac{d\sigma^{SMC}_{nn'}(E_n)}{dE_{n'}} \right] , \qquad (24a)$$

as well as,

$$\sigma_{n,p\gamma}(E_n) = \int_{x_2}^{E_{max}} dE_p \left[\frac{d\sigma_{n,p}(E_n)}{dE_p} \right] . \qquad (24b)$$

where $x_1 = \max\{0, E_n - B_{2n} - A_{3,2}\}$, $x_2 = \max\{0, E_{max} - B_{2n} - A_{3,2}\}$, and $E_{max} = E_n + B_n - B_p$. The minimum Pauli-correction energy is chosen here for the exciton state n=5 and is called $A_{3,2}$. Below MPE threshold, $E_n \leq B_n + A_{3,2}$ ($E_{max} \leq B_n + A_{3,2}$), we have $\sigma_{n,n'\gamma} = \sigma_{n,n'}$ ($\sigma_{n,p\gamma} = \sigma_{n,p}$) and, thus, we obtain from (23) the required form $\sigma^{MPE}_{n,n'} \equiv 0$ ($\sigma^{MPE}_{n,p} \equiv 0$). Notice the occurence of the SMD-term in (24a). Here, the assumption was made that in non-rearrangement direct processes (i.e. processes where the incident and outgoing particle is the same) the target deexcitation proceeds completely via γ-emission. In Fig.1 a schematic representation of $\sigma_{n,n'\gamma}(E_n)$ according to (24a) is presented.

A comment about the mean life times τ_m seems approriate. Comparing the calculated τ_m at equilibrium stage $\bar{m}$ for the first-chance emission, $\tau^{(1)}_{\bar{m}}$, with the same quantity for the second-chance emission, $\tau^{(2)}_{\bar{m}}$, the relation $\tau^{(2)}_{\bar{m}}/\tau^{(1)}_{\bar{m}} \simeq 10^3 \ldots 10^4$ holds. Physically, this demonstrates the well-known fact that the the second-chance particle b will be emitted $10^3 \ldots 10^4$ timeslater than the first-chance particle c.

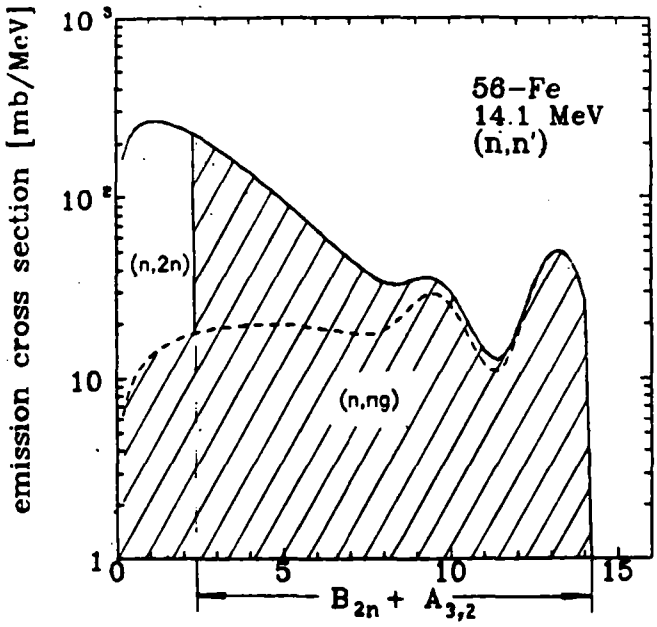

Fig.1 SMD plus SMC emission cross section with MPE threshold. The dashed area represents the $(n,n\gamma)$ cross section; the white area is the MPE cross section (n,2n) plus (n,np). For denotations see text

In summary, the above MPE model combines both the ideas of multistep theory (introduction of exciton number) and the simplicity of older models in performing calculations (short computer running time). Especially the latter plays an important role for evaluation of higher-chance emission processes (e.g., particle-deexcitation of fission fragments [18]).

III. Results and conclusions

To test the above model calculations will be presented for different groups of nuclei: even-even targets (^{48}Ti, ^{52}Cr, ^{56}Fe, ^{60}Ni), even-odd targets (^{59}Co, ^{65}Cu), and odd-even targets (^{47}Ti). Further the even-even target ^{58}Ni is chosen as a representative

for a magic nucleus. Besides (n,p) and (n,2n) activation cross sections also neutron and proton emission spectra at 14 MeV incident energy are shown together with experimental data.

The calculations are performed by code EXIFON [19] on AT personal computer (750 lines; 100 kByte). The running time for one full-scale description per nucleus (which includes all activation cross sections plus emission spectra from zero up to 20 MeV incident energy) strongly depends on the incident-energy bin ΔE_α. For example, for ΔE_α= 1 MeV, 0.2 MeV we have computer running times of about 100 secs and 7 min, respectively.

The input for the calculations are the experimental binding energies of Wapstra and Bos [20] as listed in mass table [12]. Then, the liquid drop binding energies are obtained from (1) with $\Delta = 12.8\ A^{-1/2}$. (The only exception is ^{48}Ti where strong deviations from this approximation are observed. Hence the values $\Delta_n = (B_n^{LD} - B_n) = 0.66$ MeV and $\Delta_p = -(B_p^{LD} - B_p) = 1.07$ MeV are taken from mass table [12].)

The OM reaction cross sections are used for the calculation of the normalization constant in (13) as well as for the penetration factors (12). Here, a simple parametrization [21] was adopted for global OM parameter sets (Wilmore-Hodgson [22] for neutrons; Perey [23] for protons). In some cases also the parametrization [21] for other proton global OM parameter sets are used (Becchetti-Greenlees [24] for ^{47}Ti, ^{59}Co, ^{60}Ni; and Menet et al. [25] for ^{58}Ni).

The (n,p) activation cross sections are depicted in Figs.2a-i for all 8 nuclei. The meaning of the curves is the same in Figs.2a-g:

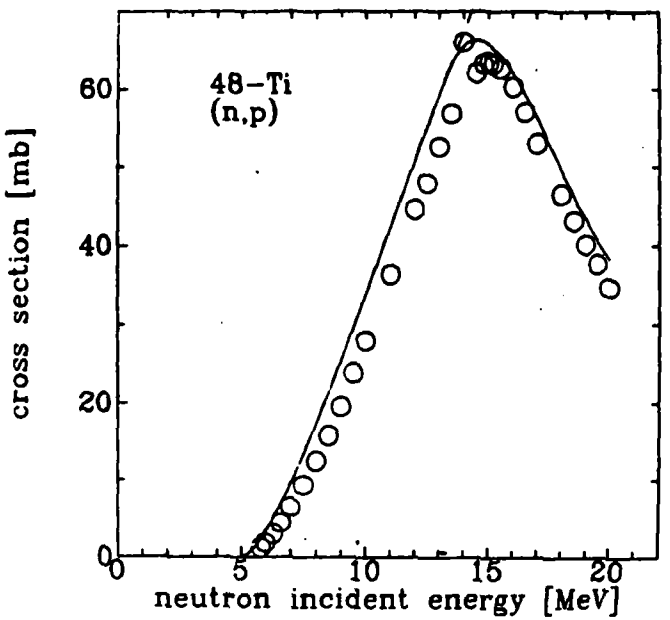

Fig.2a

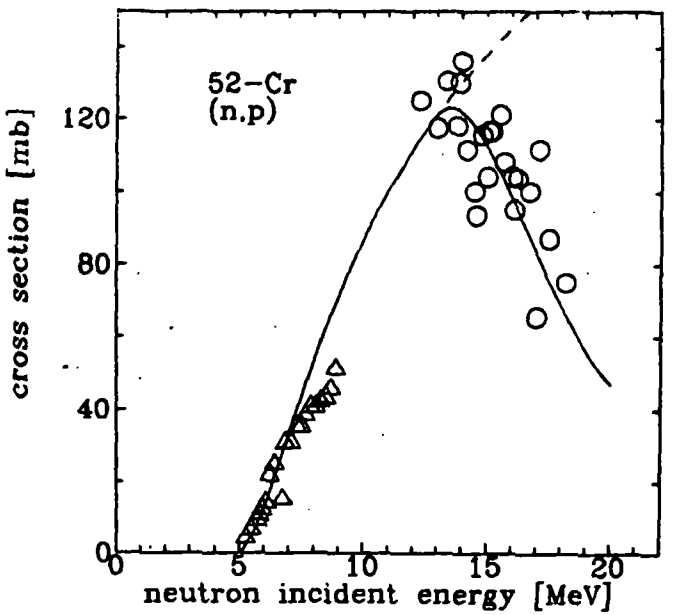

Fig.2b

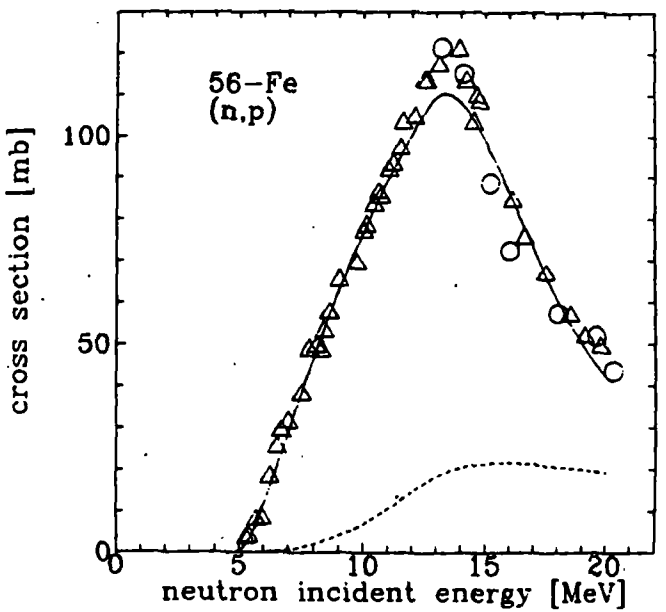

Fig.2c

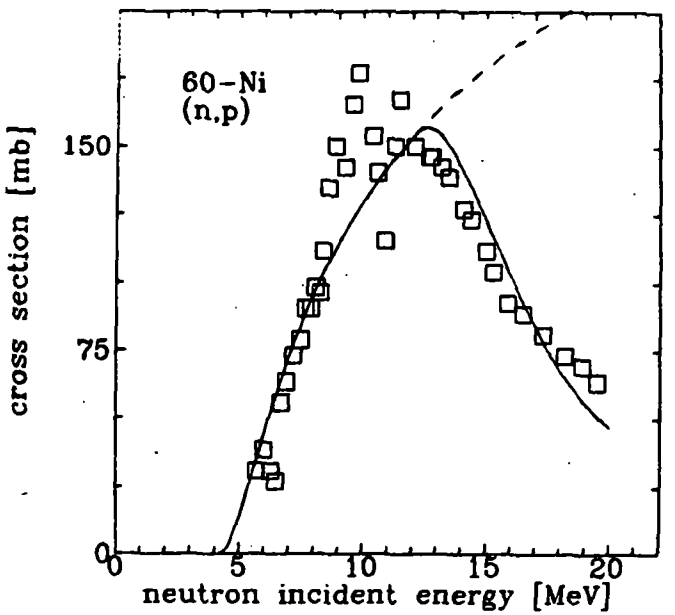

Fig.2d

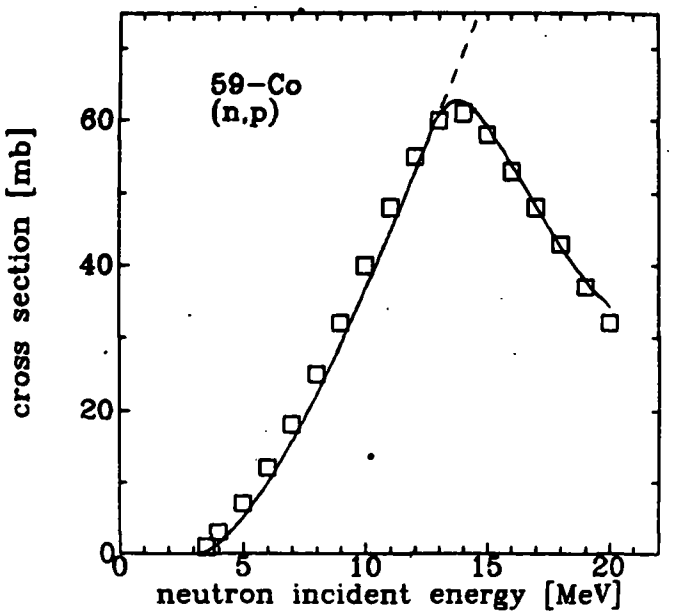

Fig.2e

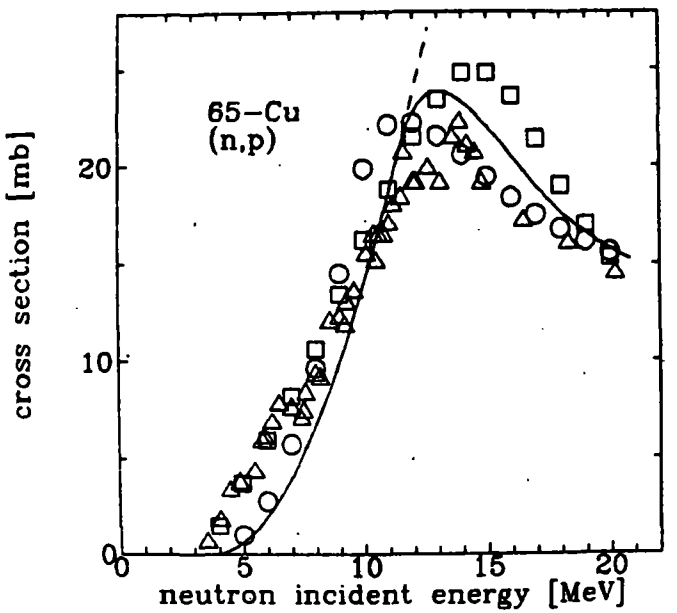

Fig.2f

Fig.2a (n,p) activation cross section. For denotations see text. Symbols represent evaluated data from [34]

Fig.2b Same as Fig.2a. Experimental data from [26] (circles) and from [27] (triangles)

Fig.2c Same as Fig.2a. Experimental data from [28] (circles) and from [29] (triangles)

Fig.2d Same as Fig.2a. Experimental data from [30]

Fig.2e Same as Fig.2a. Symbols denote evaluated data from [35]

Fig.2f Same as Fig.2a. Experimental data from [31] (circles) and from [32] (triangles). Evaluated data from [35] (squares)

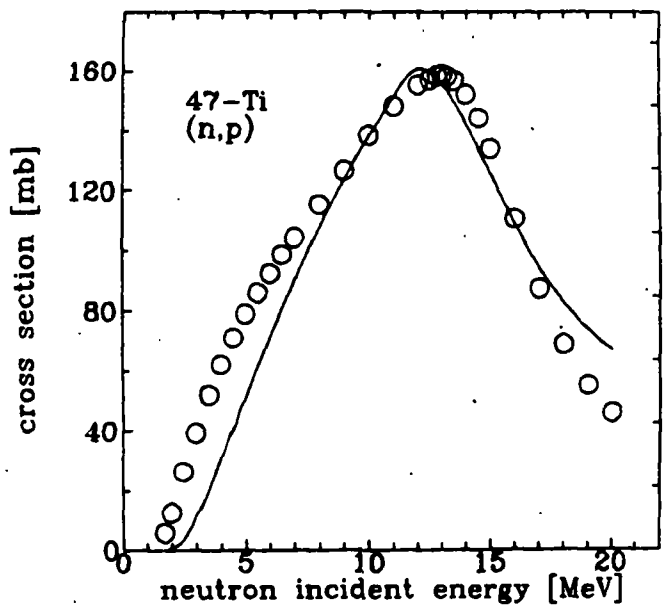

Fig.2g

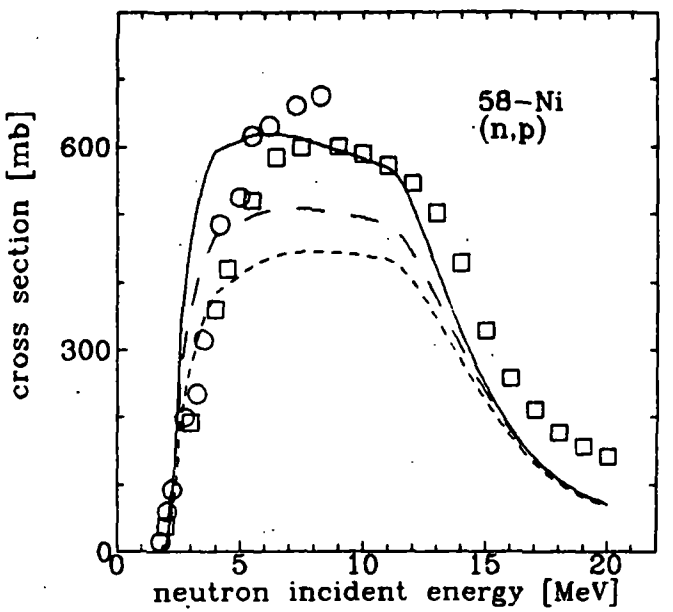

Fig.2h

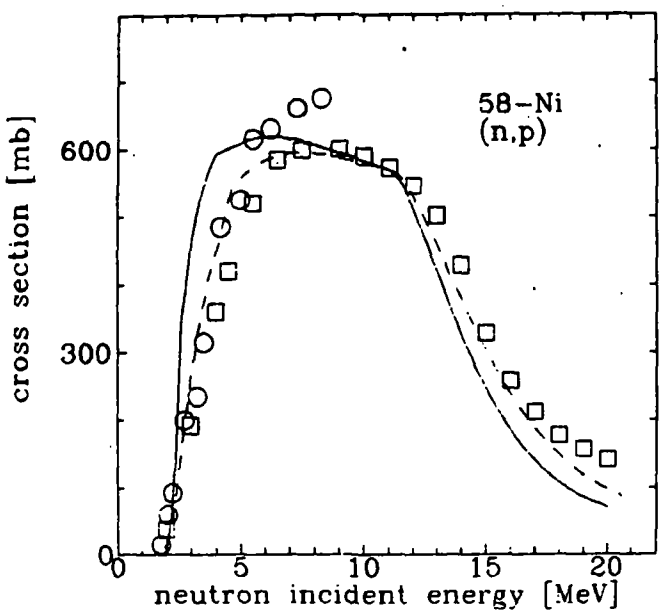

Fig.2i

Fig.2g Same as Fig.2a.

Fig.2h Same as Fig.2a. Experimental data from [33] (circles); evaluated data from [35] (squares)

Fig.2i Same as Fig.2h. Variation of g-parameter

broken lines denote $\sigma_{n,p}(E_n)$, whereas the activation cross section $\sigma_{n,p\gamma}(E_n)$ which is defined in (6a) is shown as full line. The latter are compared with experimental [26-33] and/or evaluated data [34,35]. The error-bars are compatible with the size of the symbols.

The (n,p) activation cross section can be discussed in two parts: below and above MPE threshold. The energy part below MPE threshold is sensitive to prove the (first-chance) SMC description (e.g., threshold behaviour, competition between neutron and proton emission, etc.). Here, besides the proton OM potential set the (n,p) cross section is principally determined by the values of binding energies. More precisely, the copetition between neutron and proton emission is controled by the escape widths (16) which due-to (17) are strongly depend (power law) on the residual excitation energy U. Thus, small differences of the latter caused by distinct neutron and proton binding energies in (18b) lead to essential deviations between neutron and proton emission cross sections. The difference between binding energies, for example in even-even targets, can also be increased by introducing a pairing shift Δ, or, which is the same, by using liquid drop binding energies (1). Comparisons between calculated and experimental data for even-even targets (see Figs.2a-d and 2h) justify the application of liquid drop binding energies. On the other hand, SMC-calculations with exact binding energies (small difference between B_n and B_p) predicts (n,p) cross sections for even-even targets which are several times smaller (see the dotted line in Fig.2c). The effect of using liquid drop binding energies for odd-mass targets is not so pronounced.

The enrgy part above MPE threshold give us a hint for the magnitute of (n,pn) cross section and proves the simple ansatz (24b). Here, in comparison with (n,pn) the (n,2p) cross section is very small (for example, $\sigma_{n,2p}$= 1.3 mb and $\sigma_{n,pn}$= 119.5 mb for ^{52}Cr at E_n= 20 MeV) and thus can be neglected. (Notice that $\sigma_{n,pn}$ can not been analyzed in neutron emission spectra (n,xn) since it is always overwhelmed by the greater (n,2n) cross section.). The maximum of the (n,p) activation cross-section curves can be used to determine the energy cut x_2 in (24b). It was found that for even-odd targets (^{65}Cu and ^{59}Co) the correction $A_{9,2}$ in x_2 should be replaced by Δ and 2Δ, respectively.

Variations of the global OM parameter set for protons are illustrated in Fig.2h. Here, the tendency is always the same: the Perey OM potential (short-dashed line) predicts the smallest (n,p) cross section; the Menet et al. OM potential (full line) gives the greatest (n,p) cross section whereas the Becchetti-Greenlees OM potential (broken line) lies in between.

The influence of the single-particle level density parameter g is demonstrated in Fig.2i. The full curve represents calculations for g=A/13; the dashed curve is for g=A/18. On the basis of this example, one may fairly conclude that in magic nuclei the better description is achieved by a smaller value of g rather than the global parameter g=A/13.

The calculated (n,2n) activation cross sections for ^{52}Cr, ^{56}Fe, ^{59}Co, and ^{65}Cu are depicted in Figs.3a-d. There is a good agreement with experimental [36,37] and evaluated data [35]. Deviations from experimental data are observed only for

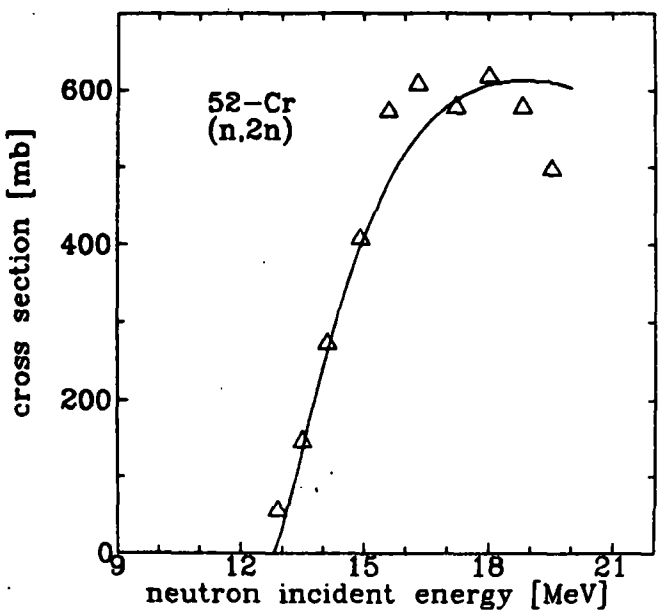

Fig.3a

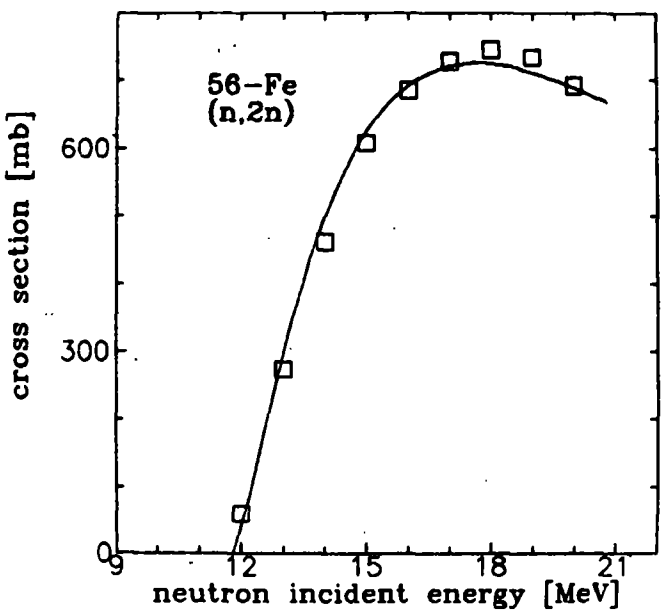

Fig.3b

Fig.3a (n,2n) activation cross section. Experimantel data from [36]

Fig.3b Same as Fig.3a. Symbols denote evaluated data from [35]

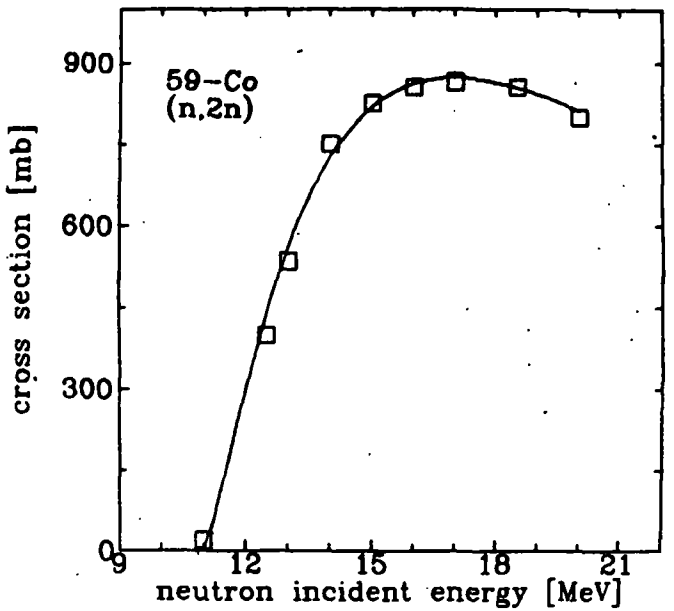

Fig.3c

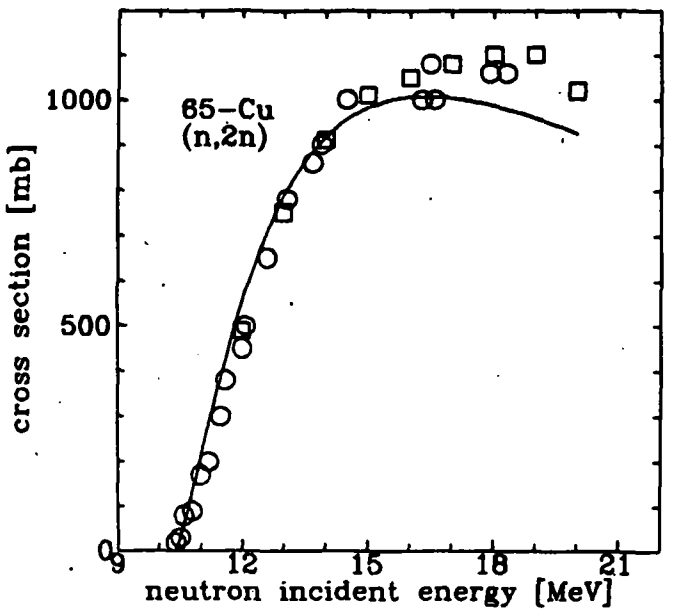

Fig.3d

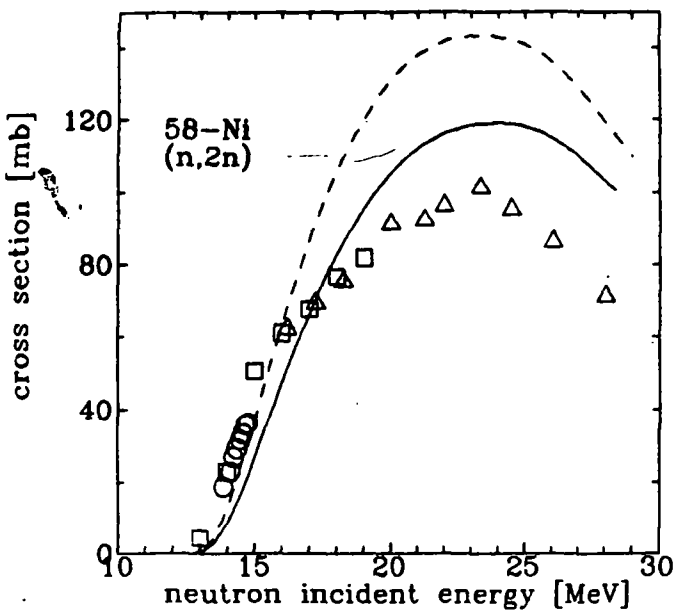

Fig.3e

Fig.3c Same as Fig.3a. Symbols denot evaluated data from [35]

Fig.3d Same as Fig.3a. Experimental data from [37] (circles); evaluated data from [35] (squares)

Fig.3e Same as Fig.3a. Experimental data from [38] (circles) and from [39] (triangles). Evaluated data from [35] (squares)

Ni-isotopes [35,38,39] where the calculations predict (several times) too high values for $E_n \geq$ 16 MeV. The situation can be improved for these isotopes if B_{2n}^{LD} is replaced by $B_{2n}^{LD}+\Delta$ which deminishes the (n,2n) and increases the (n,np) cross sections. The obtained result for ^{58}Ni is shown in Fig.3e where the parameters g=A/13 (full line) and g=A/18 (dashed line) are used. Here the big discrepancy is reduced but again, the calculations overpredict the experimental data. This is due-to the relatively high α-emission probability for Ni-isotopes (about 100 mb at E_n= 14 MeV) which is ignored in our calculation.

To complete the discussion we present finally the neutron and proton emission spectra at 14 MeV incident energy in Figs.4a-e and 5a-e. Here the following denotation is used: SMC cross sectio (broken line), SMC plus SMD cross sections (short dashed line), and the total emission spectrum including MPE (full line). In Figs.4a-e the experimental [40,41] and calculated (n,xn) spectra coincide surprisingly well despite the graet simplicity of the model. (Small overpredictions in the calculations for ^{48}Ti and ^{58}Ni are mainly due-to the missing of α-competition). The two bumbs in the high-energy tail are caused by direct phonon excitations of multipolarity 2^+ and 3^- named by [vib] in our SMD description. Notice that the experimental data of Baba et al. [41] (crosses) include also the elastical peak.

There is also fair agreement between experimental [34,42] and calculated (n,xp) cross secttions for the same nuclei. Notice that the proton spectra of ^{65}Cu is about one order of magnitude smaller than those from the ligther even-even targets.

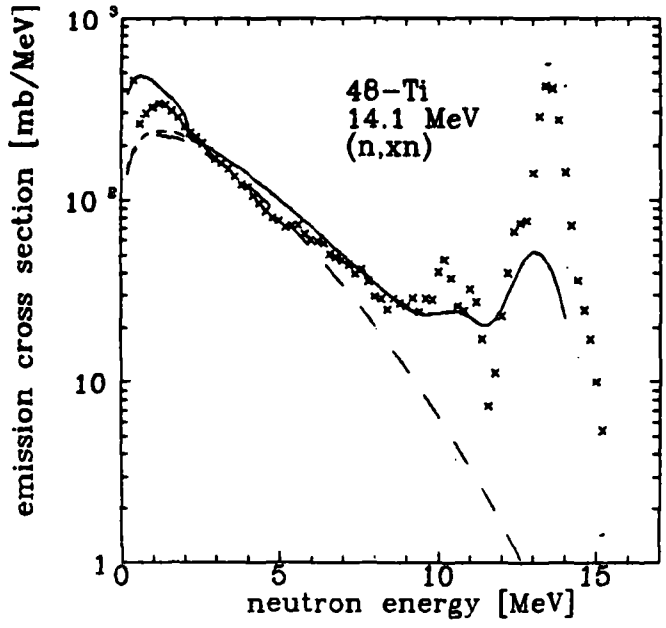

Fig.4a Neutron emission cross section at 14.1 MeV incident energy. Experimental data from [40] (circles) and from [41] (crosses). For denotations see text

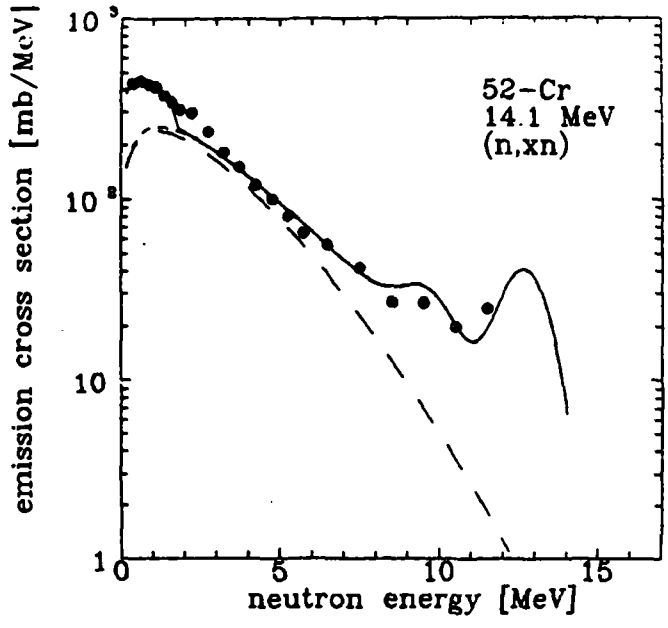

Fig.4b Same as Fig.4a

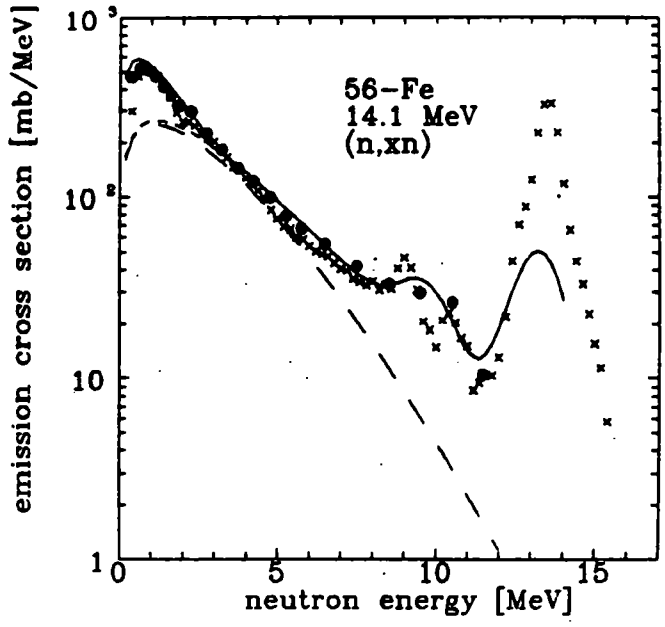

Fig.4c Same as Fig.4a

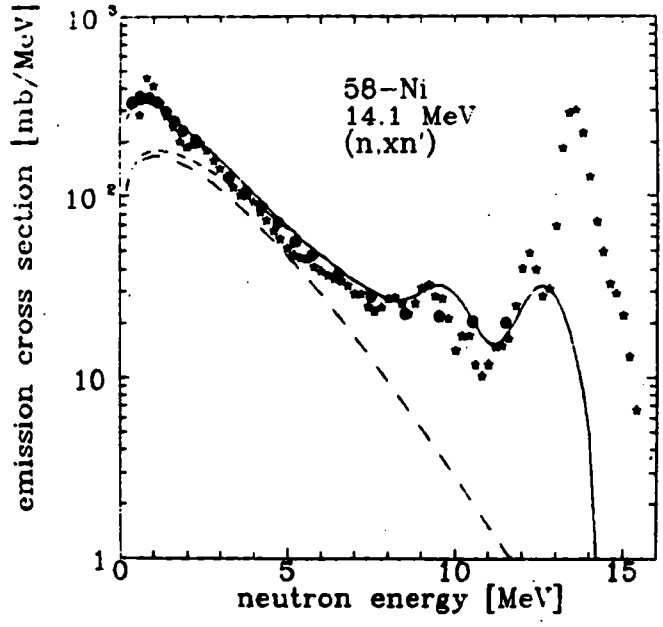

Fig.4d Same as Fig.4a

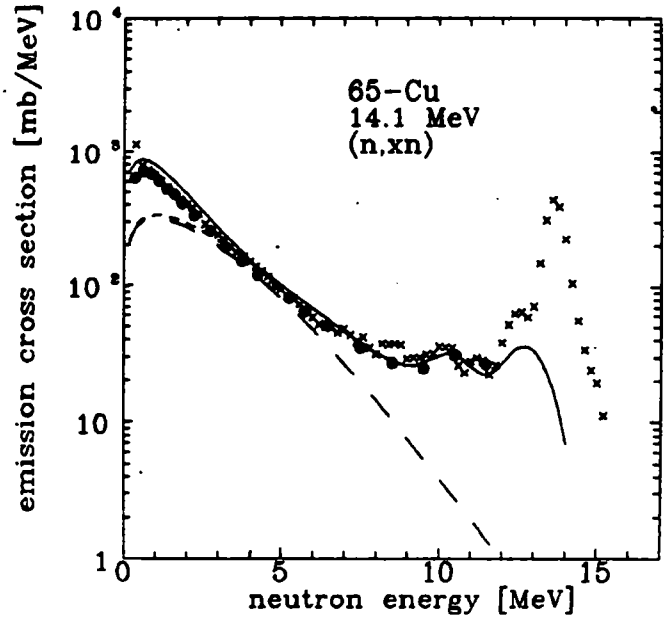

Fig.4e Same as Fig.4a

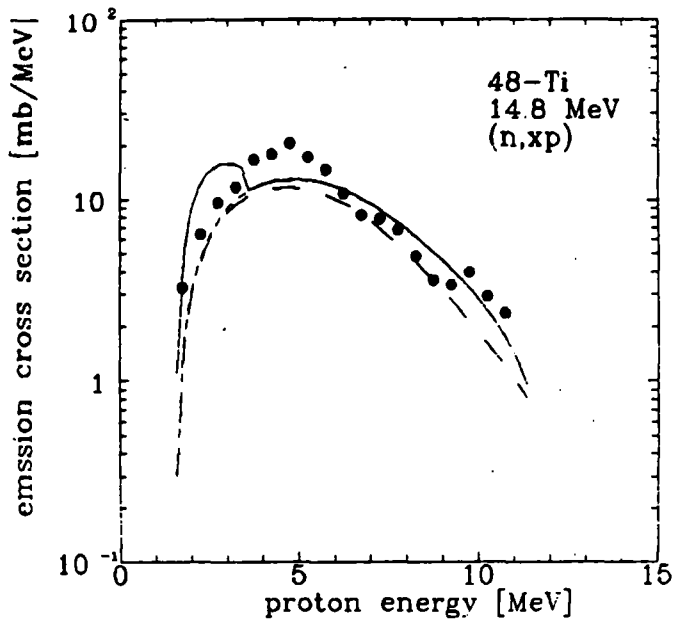

Fig.5a Proton emission cross section at 14.8 MeV incident energy. Experimental data from [34]. For denotations see text.

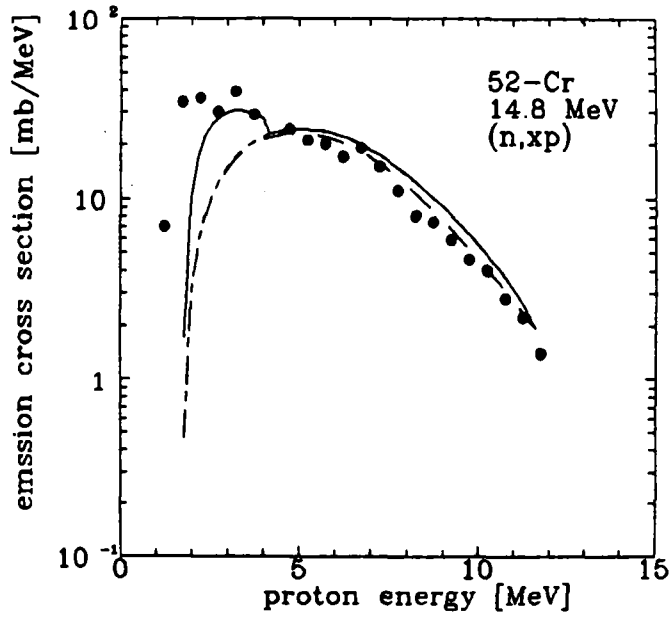

Fig.5b Same as Fig.5a. Experimental data from [42]

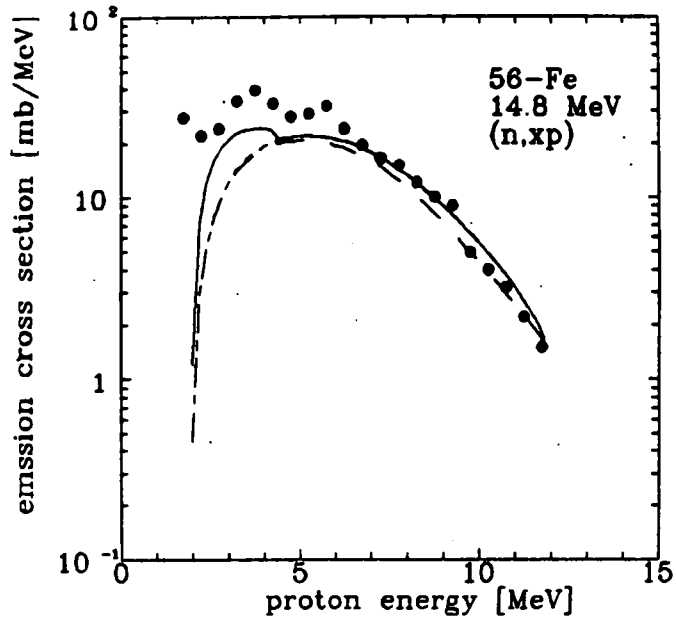

Fig.5c Same as Fig.5a.

Experimental data from [42]

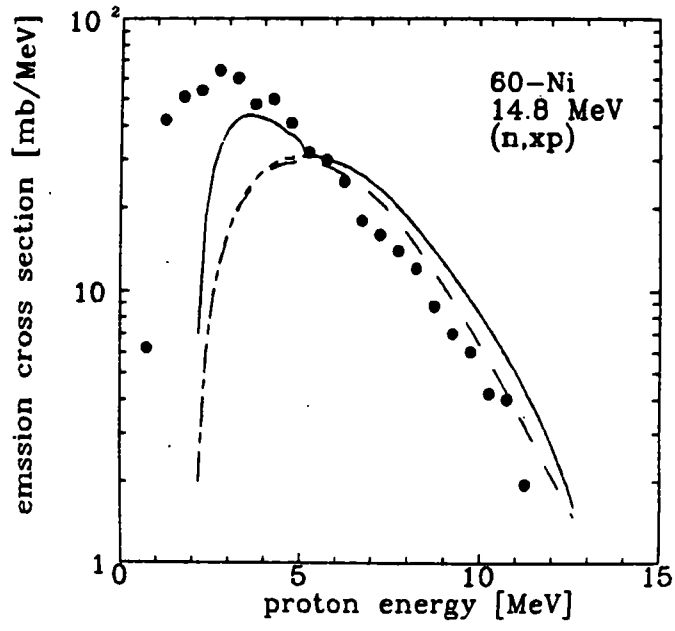

Fig.5d Same as Fig.5a.

Experimental data from [42]

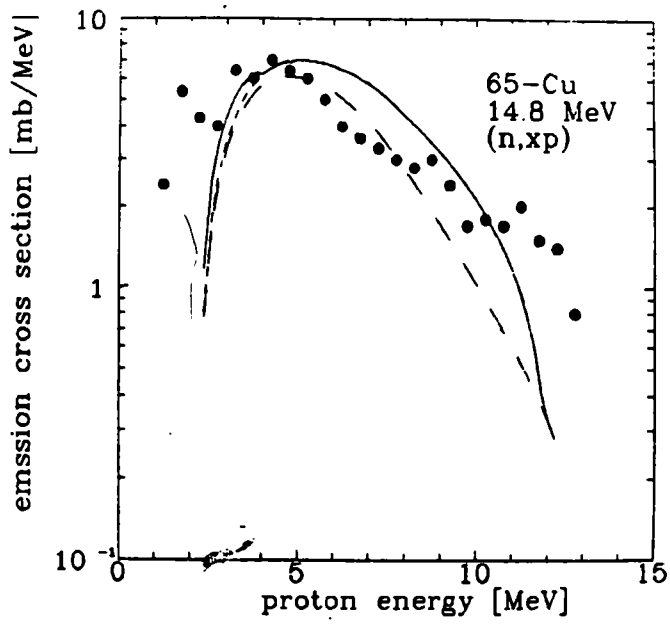

Fig.5e Same as Fig.5a.

Experimental data from [42]

In summary, the above statistical multistep model is succesful in reproducing activation cross sections as well as emission spectra by using only global parameters. Special care is only required for magic nuclei, i.e., ^{58}Ni. Starting out from this global and/or standard describtion this model seems appropriate for further improvements and investigations.

References

1. Meister,A., Seeliger,D., Seidel,K.: Kernenergie **12**, 39 (1977)
2. Holub,E., Pocanic,D., Caplar,R., Cindro,N.: Phys.Rev.C **28**, 252 (1983)
3. Ivascu,M. ,Avrigeanu,M., Ivascu,I., Avrigeanu,V.: INDC (ROM)-020/LJ (1980)
4. Garg,S.B.: INDC(IND)-041/LJ (1989)
5. Kalka,H., Seeliger,D., Zhivopistsev,F.A.: Z.Phys.A **329**, 331 (1988)
6. Kalka,H., Torjman,M., Seeliger,D.: submitted to Phys.Rev.C
7. Agassi,D., Weidenmüller,H.,A., Mantzouranis,G.: Phys.Rep.**22**, 145 (1975)
8. Brody,T.A., Flores,J., French,J.B., Mello,P.A., Pandey,A., Wong ,S.M.: Rev.Mod.Phys. **53**, 385 (1981)
9. Zhivopistsev,F.A., Sukharevsky,V.G.: Phys.Elem.Particle.and Nuclei, Dubna **15**, 1208 (1984)
10. Kalka,H.: in *Proceedings of the Workshop on Applied Nuclear Theory and Nuclear Model Calculations for Nuclear Technology*, Trieste 1988, in print
11. Kalka,H., Seeliger,D.: in *Proceedings of the 5th Symposium on Nuclear Induced Reactions* , Smolenice 1988, in print
12. Ando,Y., Uno,M., Yamada,M.: JAERI-M83-025 (1983)

13. Dilg,W., Schantl,W., Vonach,H., Uhl,M.: Nucl.Phys.A **217**, 269 (1973)

14. Bohr,A., Mottelson,B.R.: Nuclear Structure Vol II (Benjamin Reading, 1975)

15. Raman,S., Malarkey,C.H., Milner,W.T., Nestor,C.W., Stelson,P.H.: At. Data and Nucl. Data Tables **36**, 1 (1987)

16. Bernstein,A.M.: Advances in Nuclear Physics, Vol **3** ,p.325 (Plenum Press, 1969)

17. Feshbach,H., Kerman,A., Koonin,S.E.: Ann.Phys.(N.Y.) **125**, 429 (1980)

18. Arnold,K., Düring,I., Kalka,H., Märten,H., Ruben,A., Seeliger,D.: in *Proceed. Int. Conf. 50 years Research in Fission*, Berlin (West) 1989, to be published

19. Kalka,H.: Code EXIFON, unpublished

20. Wapstra,A.H., Bos,K.: At. Data and Nucl. Data Tabels **19**, 175 (1977)

21. Chatterjee,A., Murthy,K.H.N., Gupta,S.K.: Pranama **16**, 391 (1981)

22. Wilmore,D., Hodgson,P.E.: Nucl.Phys. **55**, 673 (1964)

23. Perey,F.G.: Phys.Rev. **131**, 745 (1963)

24. Becchetti,F.D., Greenlees,G.W.: Phys.Rev.**182**, 1190 (1969)

25. Menet,J.J.H., Gross,E.E., Malanify,J.J., Zucker,A.: Phys.Rev. C **4**, 1114 (1971)

26. Kreger,W., Hern,B.D.: Phys.Rev. **113**, 980 (1969)

27. Smith,D.L., Meadows,J.W.: Nucl.Sci.Eng. **76**, 34 (1981)

28. Bormann,M., Cierjacks,S., Langkau,R., Neuert,H.: Z.Phys.**166**, 477 (1962)

29. Santry,D.C., Butler,J.P.: Can.J.Phys. **42**, 1030 (1964)

30. Paulsen,A.: Nukleonik **10**, 91 (1967)

31. Bayhurst,B.P., Prestwood,R.J.: J. Inorg. Nucl. Chem. **23**, 173 (1961)

32. Santry,D.C., Butler,J.P.: Can.J.Phys. **44**, 1183 (1966)

33. Barry,J.: J.Nucl.Energy AB **16**, 467 (1962)

34. DayDay,N., Lemmel,H.D., Pronyaev,V.G.: ENDF/B-5 *(Revision 2) Dosimetry File* , IAEA-NDS-24 (1984)

35. Manokhin,V.N., Pashchenko,A.B., Plyaskin,V.I., Bychkov,V.M., Pronyaev,V,G.: in *Hand Book on Nuclear Activation Data*, p.305 (1987)

36. Bormann,M., Behrend,A., Riehle,I., Vogel,O.: Nucl.Phys.A **115**, 309 (1968)

37. Nagel,W., Aten,A.H.W.: Jr.Physica **31**, 1091 (1965)

38. Glaver,R.N., Weigold,E.: Nucl.Phys. **29**, 309 (1962)

39. Bayhurst,B.P., Gilmore,J.S., Prestwood,R.J., Wilbhny,J.B., Erkkila,B.H., Hardekopf,R.A.: Phys.Rev. C **12**, 451 (1975)

40. Pavlik,A., Vonach,H.: *Evaluation of the Angle Integrated Neutron Emission Cross Sections from the Interaction of 14 MeV with Medium and Heavy Nuclei* ,IRK-Report, Vienna ,1988

41. Baba,M., Ishikawa,M., Yabuta,N., Kikuchi,T., Wakabayashi,H., Hirakawa,N.: *Int Conf.on Nuclear Data for Sciens and Technolgy*, Mito 1988

42. Grimes,M., Haight,R.C. ,Alvar,K.R., Barschall,H.H., Borchers,R.R.: Phys.Rev.C **19**, 2127 (1979)